Arabian Journal of Chemistry (2020) 13, 974–987

King Saud University

Arabian Journal of Chemistry

www.ksu.edu.sa
www.sciencedirect.com

ORIGINAL ARTICLE

Synthesis and special characterization through X-ray analysis of 1,8-dioxooctahydroxanthenes

Milene Lopes da Silva [a], Róbson Ricardo Teixeira [a,*], Lucas de Azevedo Santos [b], Felipe Terra Martins [c], Teodorico Castro Ramalho [b]

[a] *Chemistry Department, Universidade Federal de Viçosa, CEP 36570-900 Viçosa, MG, Brazil*
[b] *Department of Chemistry, Federal University of Lavras, CEP 37200-000 Lavras, MG, Brazil*
[c] *Chemical Institute, Federal University of Goiás, CEP 74001-970 Goiânia, GO, Brazil*

Received 22 January 2017; accepted 2 September 2017
Available online 9 September 2017

KEYWORDS

1,8-Dioxooctahydroxanthenes;
X-ray analysis;
DFT calculations

Abstract Pyran moiety containing heterocyclic compounds have the capability for binding to either side to cyclohex-2-enone rings and to form xanthene derivatives (1,8-dioxooctahydroxanthenes also known as xanthenodiones). These xanthene derivatives display a wide range of biological activities and find applications in laser technologies and photodynamic therapy. This paper describes the preparation, X-ray structural analysis, and theoretical investigation of a series of 1,8-dioxooctahydroxanthenes. The compounds were synthesized via Knoevenagel condensation between different aldehydes and β-diketones. The reactions were performed free of solvents and the 1,8-dioxooctahydroxanthenes were obtained in good yields (70–92%). All the compounds were fully characterized by NMR and IR spectroscopy as well as mass spectrometry. Among the synthesized compounds, seven had their crystal structures elucidated for the first time. In all the new crystal structures, the three fused rings did form an almost completely planar xanthenodione core, except for the side rings that adopt half-chair conformation with both carbons at the flaps oriented toward to the aromatic substituent, or with one of the two carbons pointing opposite to the substituent. Another conformational difference among the new compounds investigated by X-ray diffraction resides in the rotation around the bond axis connecting the xanthenodione core to its aromatic substituent. It was found that different bent levels resulted from weak intermolecular contact patterns. In addition, theoretical calculations for single molecule and dimmers have provided insights into the balance between intramolecular and intermolecular forces driving both conformational features.

* Corresponding author.
E-mail address: robsonr.teixeira@ufv.br (R.R. Teixeira).
Peer review under responsibility of King Saud University.

ELSEVIER Production and hosting by Elsevier

1. Introduction

The heterocyclic compounds are of great importance in the realm of organic chemistry. They abound in nature and natural heterocycles present a broad range of important biological activities (Quin and Tyrell, 2010). Several agrochemicals and

https://doi.org/10.1016/j.arabjc.2017.09.001
1878-5352

pharmaceuticals bear heterocycle functionalities in their structures (Dua et al., 2011; Lamberth and Dinges, 2012a,b). Heterocycles are also an integral part of several dyes, luminophores and polymers. Oxygen and nitrogen containing compounds constitute the largest and most varied group of heterocycles.

Xanthene (9*H*-xanthene, 10*H*-9-oxaanthracene) is an oxygenated heterocyclic endowed with fungicidal activity (Obi-Egbebi and Obot, 2012). Several xanthene-based dyes, such as fluorescein, eosins, and rhodamines are known. These dyes have several uses in textiles, paper, food, cosmetics, pharmaceuticals, medicine, and biological staining due to their superior dyeing and coloring properties. In addition to the dyes, other important xanthene derivatives are well known (Pirouzmand et al., 2017; Kalantari, 2012; Banerjee et al., 2016; Ziarani et al., 2011; Naidu et al., 2012).

Heterocyclic compounds containing a pyran nucleus fused on either side with cyclohex-2-enone rings are collectively called 1,8-dioxooctahydroxanthenes (also known as xanthenodiones). These xanthene derivatives display broad biological activities including antifungal (Omolo et al., 2011), antibacterial (Wang et al., 2006), anti-inflammatory (Poupelin et al., 1978), leishmanicidal (Nisar et al., 2013), and antitumor (Mulakayala et al., 2012). In addition, these compounds are found in cosmetics and pigments (Ilangovan et al., 2011), biodegradable agrochemicals (Hafez et al., 1987), and fluorescent materials (Callan et al., 2005). Xanthenodiones also find applications in laser technologies (Banerjee and Mukherjee, 1981) and photodynamic therapy (Ion et al., 1998). All these biological activities and applications have attracted the attention of researchers to this class of compounds.

We have been interested in the preparation and investigation of biological properties of 1,8-dioxooctahydroxanthenes. Within this context, we were able to obtain monocrystals of several prepared 1,8-dioxooctahydroxanthenes. Considering that the knowledge of structural aspects is important in terms of structure-activity relationship, we undertook the task of investigating structural aspects of several xanthenodiones.

In this paper, we describe the synthesis of a series of nine xanthenodiones and the results of a comparative investigation of their crystal structures. The crystal structures of seven derivatives are described for the first time. Theoretical aspects associated with these compounds are also discussed.

2. Experimental

2.1. Generalities

All reagents were purchased from commercial sources (Sigma Aldrich - St. Louis, MO, US and Vetec - Rio de Janeiro, Brazil) and were employed as received. Solvents were procured from Vetec (Rio de Janeiro, Brazil) and were used as received. The ^{1}H and ^{13}C NMR spectra were recorded on a Varian Mercury 300 instrument (300 MHz and 75 MHz respectively), using deuterated chloroform as solvent. Hydrogen nuclear magnetic resonance (NMR) data are presented as follows: chemical shift (δ) in ppm, number of hydrogen atoms, multiplicity, J values in Hertz (Hz) and assignment. Multiplicities are shown as the following abbreviations: s (singlet), d (doublet), t (triplet), m (multiplet). Infrared spectra (IR) were obtained employing the Varian 660-IR equipment with accessory GladiATR. Mass spectra were recorded on a SHIMADZU GCMS-QP5050A instrument under electron impact (70 eV) conditions. The mass was acquired in positive mode scanning from 50 to 1000 Da. Melting points were determined using MQAPF-301 melting point apparatus (Microquimica, Rio de Janeiro, Brazil). Analytical thin layer chromatography analysis was carried out on TLC plates recovered with 60GF254 silica gel.

2.2. Synthesis

2.2.1. Synthesis of 9-(4-bromophenyl)-3,3,6,6-tetramethyl-3,4,5,6,7,9-hexahydro-1H-xanthene-1,8(2H)-dione (3)

In a typical procedure, a round-bottomed flask (25 mL) was charged with 5,5-dimethylcyclohexan-1,3-dione (294.9 mg, 2 mmol), 4-bromobenzaldehyde (186.9 mg, 2 mmol) and $ZrOCl_2{\cdot}8H_2O$ (12 mg, 2 mol%). The mixture was stirred at 85 °C and the progress of the reaction was monitored by TLC analysis. After completion of the reaction, the mixture was cooled down to room temperature. Thereafter, it was added to the flask 50 ml of dichloromethane and the mixture was kept under stirring for about 30 min. Then, the catalyst, which is insoluble in dichloromethane, was separated by filtration. After that, 50 mL of ethanol was added and the system was kept undisturbed for recrystallization process. This procedure afforded compound **3** as a pale yellow solid in 80% yield (344.0 mg, 0.80 mmol). Crystals suitable for X-ray diffraction studies were obtained from the above mentioned recrystallization method. The obtained crystals were thoroughly washed with cold ethanol and dried. Structure of **3** is supported by the following data. See Fig. 1 for numbering.

White solid (344.3 mg, 0.80 mmol, 80% yield), Mp 239–240 °C. IR (ATR): 2952 (ν_{as} CH_3), 2876 (ν_s CH_3), 1659 (ν C═O), 1624 (ν C═C), 1360 (δ CH_3), 1197 (ν_{as} ═C—O—C), 1165 (skeletal vibration of CH_3), 1139 (skeletal vibration of CH_3) cm^{-1}. ^{1}H NMR (300 MHz, $CDCl_3$) δ: 7.32 (2H, d, J = 8.0 Hz, Ar—H), 7.16 (2H, d, J = 8.0 Hz, Ar—H), 4.69 (1H, s, 3-H), 2.46 (4H, s, 8-CH_2 and 11-CH_2), 2.23 (d, 2H, J = 16.5 Hz, 6-H_a and 13-H_a), 2.15 (d, 2H, J = 16.5 Hz, 6-H_b and 13-H_b), 1.09 (6H, s, 14-CH_3 and 17-CH_3), 0.98 (6H, s, 14-CH_3 and 16-CH_3). ^{13}C NMR (75 MHz, $CDCl_3$) δ: 196.3 (C1 and C5), 162.5 (C9 and C10), 156.6 (C—Ar), 143.2 (C—Ar), 131.1 (C—Ar), 130.2 (C—Ar), 120.2 (C—Ar), 115.1 (C2 and C4), 50.7 (C6 and C13), 40.8 (C8 and C11), 32.2 (C3), 31.5 (C7 and C12), 29.3 (C15 and C16), 27.3 (C14 and C17). MS, m/z (%): 430 (M + 2, 30), 428 ($C_{23}H_{25}BrO_3$, M^+, 30), 349 (21), 273 (100), 217 (26), 161 (17), 55 (22), 41 (31).

2.2.2. Synthesis of 4–11

A similar procedure to that described for the preparation of **3** was utilized to synthesize compounds **4**–**11**. The structures of these compounds are supported by the following data.

2.2.2.1. 9-(4-Clorophenyl)-3,3,6,6-tetramethyl-3,4,5,6,7,9-hexahydro-1H-xanthene-1,8(2H)-dione (4). White solid (324.1 mg, 0.84 mmol, 84% yield), Mp 232–233 °C. IR (ATR): 2951 (ν_{as} CH_3), 2875 (ν_s CH_3), 1659 (ν C═O), 1624 (ν C═C), 1360 (δ CH_3), 1196 (ν_{as} ═C—O—C), 1164 (skeletal vibration of CH_3), 1139 (skeletal vibration of CH_3) cm^{-1}. ^{1}H NMR (300 MHz, $CDCl_3$) δ: 7.22 (2 H, d, J = 7.9 Hz, Ar—H), 7.17 (2H, d, J = 7.9 Hz, Ar—H), 4.70 (1H, s, 3-CH), 2.46 (4H,

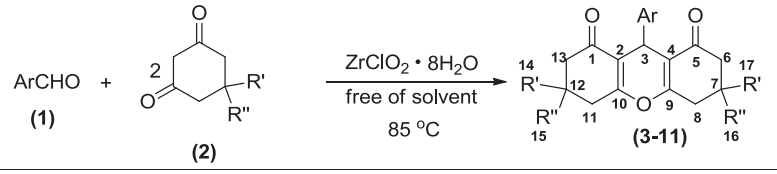

Compound	Ar	R'/R''	Reaction Time (min)	Yield (%)
3	4-bromophenyl	R'=R''=methyl	60	80
4	4-chlorophenyl	R'=R'' =methyl	30	84
5	4-chlorophenyl	R'=H; R"= methyl	20	80
6	5-(4-bromophenyl) furan-2-yl	R'=H; R"=H	120	75
7	5-(4-chlorophenyl) furan-2-yl	R'=H; R"=H	120	78
8	5-phenyl-thiophene-2-yl	R'=H; R"=H	50	92
9	4-dimethylaminophenyl	R'=H; R"=H	60	70
10	4-fluorophenyl	R'=R''=methyl	60	80
11	5-phenyl-thiophen-2-yl	R'=R''=methyl	50	94
12	phenyl [i]	R'=R''=methyl	-	-

Fig. 1 Synthesis of xanthenodiones **3**–**11**. [i] Compound **12** was not synthetized in this study even though its geometry is key to understand the xanthenodione structures.

s, 8-C$\underline{H}_2$ and 11-C$\underline{H}_2$), 2.23 (2H, d, J = 16.5 Hz, 6-H_a and 13-H_a), 2.15 (2H, d, J = 16.5 Hz, 6-H_b and 13-H_b), 1.09 (6H, s, 14-C$\underline{H}_3$ and 17-C$\underline{H}_3$), 0.98 (6H, s, 14-C$\underline{H}_3$ and 16-C$\underline{H}_3$). ^{13}C NMR (75 MHz, $CDCl_3$) δ: 196.4 (C1 and C5), 162.4 (C9 and C10), 142.7 (C—Ar), 132.0 (C—Ar), 129.8 (C—Ar), 128.2 (C—Ar), 115.2 (C2 and C4), 50.7 (C6 and C13), 40.8 (C8 and C11), 32.2 (C3), 31.4 (C7 and C12), 29.3 (C15 and C16), 27.3 (C14 and C17). MS, m/z (%): 386 (M + 2, 14), 384 ($C_{23}H_{25}ClO_3$, M +, 39), 349 (16), 273 (100), 217 (28), 161 (18) 55 (23), 41 (32).

*2.2.2.2. 9-(4-Chlorophenyl)-3,6-dimethyl-3,4,5,6,7,9-hexahydro-1H-xanthene-1,8(2H)-dione (**5**).* White solid (286.8 mg, 0.80 mmol, 80% yield), Mp 226–228 °C. IR (ATR): 2962 (ν_{as} CH_2), 2876 (ν_s CH_2), 1665 (ν C═O), 1619 (ν C═C), 1185 (ν ═C—O—C). ^{1}H NMR (300 MHz, $CDCl_3$) δ: 7.23–7.14 (4H, m, Ar—H), 4.72 (1H, s, 3-CH), 2.70–2.50 (2H, m, 6-Ha e 13-Ha', m), 2.48–2.16 (6H, m, 6-Hb, 13-Hb', 8-Hc, 11-Hc', 7-CH and 12-CH), 2.09–1.97 (2H, m, 8Hd and 13Hd'), 1.13–0.99 (6H, m, 15-C$\underline{H}_3$ e 16-C$\underline{H}_3$). ^{13}C NMR (75 MHz, $CDCl_3$) δ: 196.5, 163.8 or 163.7 (C1 and C5), 163.1 or 163.0 (C9 and C10), 142.9 or 142.8 (C—Ar), 132.1 or 132.0 (C—Ar), 129.8 or 129.7 (C—Ar), 128.2 or 128.1 (C—Ar), 116.1 or 115.9 (C2 and C4), 45.2 or 45.1 (C6 and C13), 35.2 or 34.9 (C8 and C11), 31.4 or 31.2 (C3), 28.4 or 28.3 (C7), 27.9 or 27.8 (C12), 20.8 or 20.7 (C15 and C16). MS, m/z (%): 358 (M + 2, 14), 356 ($C_{21}H_{21}ClO_3$, M^+, 42), 321 (33), 245 (100), 203 (11).

*2.2.2.3. 9-(5-(4-Bromophenyl) furan-2-yl)-3,4,5,6,7,9-hexahydro-1H-xanthene-1,8(2H)-dione (**6**).* Yellow solid (310.2 mg, 0.75 mmol, 75% yield), Mp 261–262 °C. IR (ATR): 2952 (ν_{as} CH_2), 2887 (ν_s CH_2), 1653 (ν C═O), 1615 (ν C═C), 1479 (ν C═C of furan), 1198 (ν_{as} ═C—O—C), 1172 (ν_s ═C—O—C) cm^{-1}. ^{1}H NMR (300 MHz, $CDCl_3$) δ: 7.42 (2 H, d, J = 7.9 Hz, Ar—H), 7.36 (2H, d, J = 7.9 Hz, Ar—H), 6.49 (1H, s, Furan-H), 6.23 (1H, s, Furan-H), 5.03 (1H, s, 3-CH), 2.68–2.38 (8H, m, 6-C$\underline{H}_2$, 8-C$\underline{H}_2$, 11-C$\underline{H}_2$, and 13-C$\underline{H}_2$), 2.05 (4H, m, C7 and C12). ^{13}C NMR (75 MHz, $CDCl_3$) δ: 196.4 (C1 and C5), 165.1 (C9 and C10), 155.2 (C-Furan), 151.0 (C-Furan), 131.6 (C—Ar), 130.1 (C—Ar), 124.8 (C—Ar), 120.3 (C—Ar), 113.7 (C2 and C4), 108.7 (C-Furan), 106.9 (C-Furan), 36.9 (C6 and C13), 27.3 (C8 and C11), 25.5 (C3), 20.4 (C7 and C12). MS, m/z (%): 440 (M + 2, 66), 438 ($C_{23}H_{19}BrO_4$, M^+, 67), 255 (84), 217 (100), 185 (40), 155 (20), 115 (54), 66 (21), 55 (73), 41 (42).

*2.2.2.4. 9-(5-(4-Chlorophenyl) furan-2-yl)-3,4,5,6,7,9-hexahydro-1H-xanthene-1,8(2H)-dione (**7**).* Yellow solid (309.1 mg, 0.78 mmol, 78% yield), Mp 261–262 °C. IR (ATR): 2930 (ν_{as} CH_2), 2888 (ν_s CH_2), 1654 (ν C═O), 1614 (ν C═C), 1484 (ν C═C of furan), 1174 (ν_s ═C—O—C). ^{1}H NMR (300 MHz, $CDCl_3$) δ: 7.43 (2H, d, J = 8.1 Hz, Ar—H), 7.27 (2H, d, J = 8.1 Hz, Ar—H), 6.48 (1H, d, J = 2.2 Hz, Furan-H), 6.24 (1H, J = 2.2 Hz, Furan-H), 5.04 (1H, s, 3-CH), 2.67–2.35 (8H, m, 6-C$\underline{H}_2$, 8-C$\underline{H}_2$, 11-C$\underline{H}_2$, and 13-C$\underline{H}_2$), 2.09–1.99 (4H, m, C7 and C12). ^{13}C NMR (75 MHz, $CDCl_3$) δ: 196.4 (C1 and C5), 165.1 (C9 and C10), 155.1 (C-Furan), 151.0 (C-Furan), 132.3 (C–Ar), 129.7 (C–Ar), 128.7 (C–Ar), 124.5 (C–Ar), 113.7 (C2 and C4), 108.7 (C-Furan), 106.9 (C-Furan), 36.9 (C6 and C13), 27.2 (C8 and C11), 25.5 (C3), 20.3 (C7 and C12). MS, m/z (%): 396 (M + 2, 36), 394 ($C_{23}H_{19}ClO_4$, M^+, 100), 349 (20), 255 (80), 217 (92), 139 (36), 55 (25).

*2.2.2.5. 9-(5-Phenyl-thiophen-2-yl)-3,4,5,6,7,9-hexahydro-1H-xanthene-1,8(2H)-dione (**8**).* Yellow solid (345.3 mg, 0.92 mmol, 92% yield), Mp 201–202 °C. IR (ATR): 2950 (ν_{as} CH_2), 2870 (ν_s CH_2), 1659 (ν C═O), 1619 (ν C═C), 1201 (ν_{as} ═C—O—C), 1171 (ν_s ═C—O—C), 756 (ν C—S). ^{1}H NMR (300 MHz, $CDCl_3$) δ: 7.49 (2 H, d, *J* = 7.5 Hz, Ar—H), 7.29 (2 H, t, *J* = 7.3 Hz, Ar—H), 7.23–7.16 (1H, m, Ar—H), 7.05 (1H, d, *J* = 3.3 Hz, S—C═C<u>H</u>), 6.89 (1H, d, *J* = 3.3 Hz, S—C═C<u>H</u>), 5.16 (1H, s, 3-C<u>H</u>), 2.71–2.53 (4H, m, 8-C<u>H</u>$_2$ and 11-C<u>H</u>$_2$), 2.50–2.33 (4H, m, 6-C<u>H</u>$_2$ and 13-C<u>H</u>$_2$), 2.09–2.00 (4H, m, 7-C<u>H</u>$_2$ and 12-C<u>H</u>$_2$). ^{13}C NMR (75 MHz, $CDCl_3$) δ: 196.5 (C1 and C5), 164.4 (C9 and C10), 148.1 (S—C═), 142.4 (S—C═), 134.7 (C—Ar), 128.7 (C—Ar), 127.0 (S—C═<u>C</u>), 126.0 (C—Ar), 125.5 (C—Ar), 122.8 (S—C═<u>C</u>), 116.2 (C2 and C4), 36.9 (C6 and C13), 27.2 (C8 and C11), 26.5 (C3), 20.3 (C7 and C12). MS, *m*/*z* (%): 376 ($C_{23}H_{20}O_3S$, M^+, 100), 359 (30), 320 (38), 217 (50), 160 (21), 121 (24), 115 (65), 77 (37), 55 (60), 41 (41).

*2.2.2.6. 9-(4-(Dimethylamino)phenyl)-3,4,5,6,7,9-hexahydro-1H-xanthene-1,8(2H)-dione (**9**).* Yellow solid (236.0 mg, 0.70 mmol, 70% yield), Mp 231–232 °C. IR (ATR): 2944 (ν_{as} CH_2), 2869 (ν_s CH_2), 1658 (ν C═O), 1610 (ν C═C), 1356 (ν Ar—N), 1199 (ν_{as} ═C—O—C). ^{1}H NMR (300 MHz, $CDCl_3$) δ: 7.15 (2 H, d, *J* = 8.5 Hz, Ar-H), 6.62 (2 H, d, *J* = 8.5 Hz, Ar—H), 4.76 (1H, s, 3-C<u>H</u>), 2.87 (6H, s, N(C<u>H</u>$_3$)$_2$), 2.65–2.52 (4H, m, 8-C<u>H</u>$_2$ and 11-C<u>H</u>$_2$), 2.37–2.28 (4H, m, 6-C<u>H</u>$_2$ and 13-C<u>H</u>$_2$), 2.04–1.95 (4H, m, 7-C<u>H</u>$_2$ and 12-C<u>H</u>$_2$).^{13}C NMR (75 MHz, $CDCl_3$) δ: 196.6 (C1 and C5), 163.5 (C9 and C10), 149.0 (C—Ar), 133.1 (C—Ar), 128.9 (C—Ar), 117.2 (C2 and C4), 112.6 (C—Ar), 40.8 (N(CH_3)$_2$), 37.0 (C6 and C13), 30.4 (C3), 27.1 (C8 and C11), 20.3 (C7 and C12). MS, *m*/*z* (%): 337 ($C_{21}H_{23}NO_3$, M^+, 100), 320 (87), 293 (20), 281 (16), 217 (17).

*2.2.2.7. 9-(4-Fluorophenyl)-3,3,6,6-tetramethyl-3,4,5,6,7,9-hexahydro-1H-xanthene-1,8(2H)-dione (**10**).* White solid (294.0 mg, 0.80 mmol, 80% yield), Mp 227–228 °C. IR (ATR): 2957 (ν_{as} CH_3), 2872 (ν_s CH_3), 1657 (ν C═O), 1626 (ν C═C), 1360 (δ CH_3), 1222 (ν C—F), 1196 (ν_{as} ═C—O—C), 1164 (skeletal vibration of CH_3), 1139 (skeletal vibration of CH_3) cm^{-1}. ^{1}H NMR (300 MHz, $CDCl_3$) δ: 7.28–7.21 (2H, m, Ar—<u>H</u>), 6.92–6.84 (2H, m, Ar—<u>H</u>), 4.72 (1H, s, 3-C<u>H</u>), 2.46 (4H, s, 8-C<u>H</u>$_2$ and 11-C<u>H</u>$_2$), 2.23 (2H, d, *J* = 16.5 Hz, 6-H_a and 13-H_a), 2.15 (2H, d, *J* = 16.5 Hz, 6-H_b and 13-H_b) 1.09 (6H, s, 15-C<u>H</u>$_3$ and 16-C<u>H</u>$_3$), 0.98 (6H, s, 14-C<u>H</u>$_3$ and 17-C<u>H</u>$_3$). ^{13}C NMR (75 MHz, $CDCl_3$) δ: 196.4 (C1 and C5), 162.3 (C9 and C10), 161.3 (d, *J* = 242.6 Hz, C—Ar), 139.9 (d, *J* = 3.0 Hz, C—Ar), 129.8 (d, *J* = 8.0 Hz, C—Ar), 115.5 (C2 and C4), 114.8 (d, *J* = 21.2 Hz, C—Ar), 50.7 (C6 and C13), 40.8 (C8 and C11), 32.2 (C3), 31.2 (C7 and C12), 29.2 (C15 and C16), 27.3 (C14 and C17). MS, *m*/*z* (%): 368 ($C_{23}H_{25}FO_3$, M^+, 54), 273 (100), 217 (30), 161 (20), 133 (17), 95 (15), 55 (23), 41 (30).

*2.2.2.8. 3,3,6,6-Tetramethyl-9-(5-phenyl-thiophen-2-yl)-3,4,5,6,7,9-hexahydro-1H-xanthene-1,8(2H)-dione (**11**).* White solid (406.2 mg, 0.94 mmol, 94% yield), Mp 169–170 °C. IR (ATR): 2955 (ν_{as} CH_3), 2867 (ν_s CH_3), 1665 (ν C═C), 1580 (ν C═O), 1359 (δ CH_3), 1197 (ν_{as} ═C—O—C), 1164 (skeletal vibration of CH_3), 1145 (skeletal vibration of CH_3), 755 (ν C—S). ^{1}H NMR (300 MHz, $CDCl_3$) δ: 7.63 (2H, d, *J* = 7.5 Hz, Ar—<u>H</u>), 7.29–7.49 (3H, m, Ar—<u>H</u>), 7.19 (1H, d, *J* = 3.3 Hz, S-C═C<u>H</u>), 7.08 (1H, d, *J* = 3.3 Hz, S—C═C<u>H</u>), 5.27 (1H, s, 3-C<u>H</u>), 2.61 (4H, s, 8-C<u>H</u>$_2$ and 11-C<u>H</u>$_2$), 2.42 (4H, s, 6-C<u>H</u>$_2$ and 13-C<u>H</u>$_2$), 1.26 (6H, s, 15-C<u>H</u>$_3$ and 16-C<u>H</u>$_3$), 1.22 (6H, s, 14-C<u>H</u>$_3$ and 17-C<u>H</u>$_3$). ^{13}C NMR (75 MHz, $CDCl_3$) δ: 196.4 (C1 and C5), 162.9 (C9 and C10), 147.9 (S—C═), 142.3 (S—C═), 134.9 (C—Ar), 128.8 (C—Ar), 127.1 (S—C═<u>C</u>), 126.5 (C—Ar), 125.6 (C—Ar), 123.0 (S—C═<u>C</u>), 115.2 (C2 and C4), 50.9 (C6 and C13), 41.0 (C8 and C11), 32.3 (C3), 29.4 (C7 and C12), 27.6 (C15 and C16), 26.9 (C14 and C17). MS, *m*/*z* (%): 432 ($C_{27}H_{28}O_3S$, M^+, 100), 415 (11), 348 (24), 273 (20), 83 (11).

2.3. X-ray diffraction analysis

Well-shaped single crystals of xanthenodione derivatives (Fig. 1) were chosen and mounted on a κ-goniostat and exposed to X-ray beam (Mo Kα, λ = 0.71073 Å) using a Bruker-AXS Kappa Duo diffractometer with an APEX II CCD detector. X-ray diffraction experiments were carried out at room temperature (see Table 1). Data collection strategy was calculated by setting φ scans and ω scans with κ offsets using the software APEX2 (Bruker, 2012). Other crystallographic softwares were used as follows: SAINT (indexing, integration and scaling of raw data) (Bruker, 2012), SHELXL-97 (structure solving) (Sheldrick, 2008), SHELXL-97 (structure refinement) (Sheldrick, 2008) and MERCURY (Macrae et al., 2008) (structure analysis and graphical representations). Direct methods of phase retrieval were used to solve the crystal structures. All non-hydrogen atoms of asymmetric unit were promptly located from the electronic density Fourier map. The early solved model was refined by full-matrix least squares method based on F^2. In the refinements, free anisotropic and fixed isotropic thermal displacement parameters were adopted for non-hydrogen and hydrogen atoms, respectively. The isotropic thermal displacement parameters of hydrogens were 20% greater than the equivalent isotropic parameter of the bonded carbon (except those hydrogens in methyl groups which were 50%). Concerning the position of all hydrogens, bond distances and angles were stereochemically constrained according to riding model.

2.4. Computational details

The geometries of synthesized compounds (Fig. 1) were optimized at ωb97xD/6-311++** level of theory by Gaussian 09-D01 software (Frisch et al., 2009). In order to obtain the temperature effect on the electronic energy, the calculations were carried out in gas phase at 25 °C and in water at 85 °C using the PCM solvation model. The conformational preference of cyclohex-2-enone moieties in the synthesized compounds was studied enforcing their respective opposite *syn* or *anti* conformer and calculating their local energy minima and thermodynamics. The conformational preference of aromatic groups was evaluated through potential energy curves scanning the O-C-C-X dihedral angle, where X = O or S, with torsions of 45°.

Table 1 Crystal data and refinement statistics for the xanthenodiones prepared in this investigation.

Compound	5	6	7	8	9	10	11
Molecular formula	$C_{21}H_{21}ClO_3$	$C_{23}H_{19}BrO_4$	$C_{23}H_{19}ClO_4$	$C_{23}H_{20}O_3S$	$C_{21}H_{23}NO_3$	$C_{23}H_{25}FO_3$	$C_{27}H_{28}O_3S$
fw (g/mol)	356.83	439.29	394.83	376.45	337.40	368.43	432.55
Cryst syst	Monoclinic	Orthorhombic	Orthorhombic	Orthorhombic	Monoclinic	Monoclinic	Monoclinic
Space group	$C2/c$	Pbca	Pbca	Pbca	$P2_1/c$	$P2_1/c$	$P2_1/c$
Z/Z'	8/1	8/1	8/1	8/1	4/1	4/1	4/1
T (K)	296(2)	296(2)	296(2)	296(2)	296(2)	296(2)	296(2)
Unit cell dimensions							
a (Å)	21.3859(6)	13.4419(18)	13.3329(13)	24.2630(14)	9.2929(14)	6.0269(2)	12.2637(5)
b (Å)	16.0215(6)	13.8418(17)	13.8091(15)	16.2820(10)	11.3538(18)	19.6459(6)	9.6726(4)
c (Å)	10.7313(4)	20.596(3)	20.4485(18)	9.5470(5)	17.113(3)	16.7818(5)	20.0243(8)
β (°)	94.126(3)	90	90	90	99.675(6)	99.690(2)	100.546(2)
V (Å^3)	3667.4(2)	3832.1(9)	3764.9(6)	3771.5(4)	1779.9(5)	1958.68(11)	2335.20(16)
Calculated density (Mg/m^3)	1.293	1.523	1.393	1.326	1.259	1.249	1.230
Absorp. coefficient μ (mm^{-1})	0.225	2.172	0.230	0.192	0.084	0.088	0.164
θ range for data collection (°)	1.59–25.64	2.33–25.35	2.35–25.37	2.09–25.37	2.16–25.86	1.61–25.41	1.69–25.38
Index ranges							
h	−25 to 25	−11 to 16	−16 to 13	−29 to 25	−11 to 10	−7 to 6	−14 to 14
k	−19 to 19	−16 to 12	−16 to 12	−17 to 18	−10 to 13	−23 to 23	−10 to 11
l	−12 to 12	−24 to 11	−24 to 13	−11 to 11	−21 to 18	−20 to 20	−24 to 20
Data collected	14443	9776	10587	12787	15320	39593	23300
Unique reflections	3434	3438	3434	3364	3411	3590	4282
Observed reflections	2399	2132	2476	2615	2349	2317	3358
Symmetry factor (R_{int})	0.0283	0.0567	0.0273	0.0691	0.0531	0.0654	0.0487
Completeness to θ_{max} (%)	98.8	97.8	99.2	97.2	99.2	99.3	99.7
F (000)	1504	1792	1648	1584	720	784	920
Parameters refined	228	253	254	244	226	244	280
Goodness-of-fit on F^2	1.047	1.024	1.047	1.039	1.076	1.053	1.042
Final $R1$ factor for $I > 2\sigma(I)$	0.0589	0.0479	0.0422	0.0510	0.0615	0.0594	0.0467
$wR2$ factor for all data	0.1793	0.1184	0.1168	0.1441	0.1909	0.1721	0.1332
Largest diff. peak/hole (e/Å^3)	0.441/−0.294	0.574/−0.336	0.246/−0.244	0.589/−0.317	0.270/−0.213	0.196/−0.209	0.219/−0.259
CCDC deposit number	1465044	1465043	1465047	1465045	1465042	1465046	1465041

3. Results and discussion

3.1. Preparation of xanthenediones 3–11

The compounds **3**–**11** were synthesized *via* Knoevenagel condensation between different aromatic aldehydes (**1**) and β-diketones (**2**) (Mosaddegh et al., 2012). The reactions were performed free of solvents and catalyzed by $ZrOCl_2{\cdot}8H_2O$, a versatile catalyst that has been involved in several synthetically useful transformations (Baltork et al., 2007; Sangshetti et al., 2008; Bardajee, 2013). From Fig. 1, the compounds were obtained in good yields within 20 min to 2 h.

The reactions were monitored by TLC analysis. The completion of the reactions was verified by the total consumption of the aldehydes. All the 1,8-dioxooctahydroxanthenes were purified via recrystallization using dichlomethane and ethanol. The structures of the compounds were confirmed upon NMR (^{1}H and ^{13}C) and IR spectroscopy, as well as mass spectrometry. In the ^{1}H NMR spectra, the hydrogen atoms of the pyran ring was observed within the 4.70–5.27 ppm range. In the ^{13}C NMR spectra, the signals for the carbonyl groups were observed near 196 ppm. In the IR spectra, carbonyl stretching frequencies were noticed in the range 1653–1670 cm^{-1} which is compatible with a conjugated carbonyl group. The molecular formulas of the xanthenodiones were confirmed by mass spectrometry analysis. The structures of compounds **3**–**11** were also investigated by single-crystal X-ray diffraction.

3.2. Crystal structures

Crystal structures of compounds **3** and **4** have been previously elucidated (Bigdeli et al., 2007; Tu et al., 2002). Their determined unit cell metrics matched those reported in the literature confirming, therefore, all conformational and intermolecular features already described for these xanthenodiones. Crystal structures of all other compounds have not been described and thus are herein reported for the first time. Crystallographic data of these compounds are presented in Table 1.

In addition to C1, compound **5** has two stereocenters and it crystallizes in the centrosymmetric space group ($C2/c$), as expected from its achiral synthesis. In the chosen asymmetric unit, chiral carbons labeled as C8 and C12 have *S* and *R* configurations; however, the enantiomeric counterpart is also present in the unit cell. Compounds **6**–**11**, each one presenting one stereocenter, have been crystallized in the centrosymmetric space groups. The crystallographic asymmetric unit of all xan-

thenodiones is composed by just one molecule, as viewed in Fig. 2. From Fig. 2, non-hydrogen atoms are shown with their 50% probability ellipsoids and arbitrary labeling scheme. Labeling of the rings is also depicted in Fig. 2.

For all compounds reported herein, the three fused rings formed an almost completely planar xanthenodione core. However, the side rings A and C adopt a half-chair conformation with C8 and C12 carbons away from the least-squares (l.s.) planes calculated through the other five coplanar atoms. The distance of these carbons from the l.s. planes and the root-mean square deviation of the l.s. fitted atoms are shown in Table 2.

Taking a xanthenodione mean plane as reference, it is interesting to observe that the flaps C8 and C12 of both half-chairs are oriented toward the aromatic substituent in compounds **5**– **8**, and **11**, which corresponds to a *syn* conformation of cyclohex-2-enone moieties. On the contrary, in xanthenodiones **3**, **4**, and **10**, C8 points toward the aromatic substituent while C12 points to the opposite direction, which relates to an *anti*- conformation of the half chairs. This trend observed for **3**, **4**, and **10** was also noticed for xanthenodione having a *para*-carboxymethoxy phenyl group (CSD ref. code GIWZAP, reference (Kumar et al., 2014)) as well as in that bearing only one phenyl moiety (herein numbered as compound **12**; CSD ref. code VOQSEA, reference (Reddy et al., 2009)). Compound **9** also presents alternated flaps; however, C8 points opposite to the *para*-substituted phenyl ring while C12 points toward it.

Another difference among compounds **5**–**11**, which is also responsible for the conformational distinction in terms of rings A and C, corresponds to the rotation around the axis of the

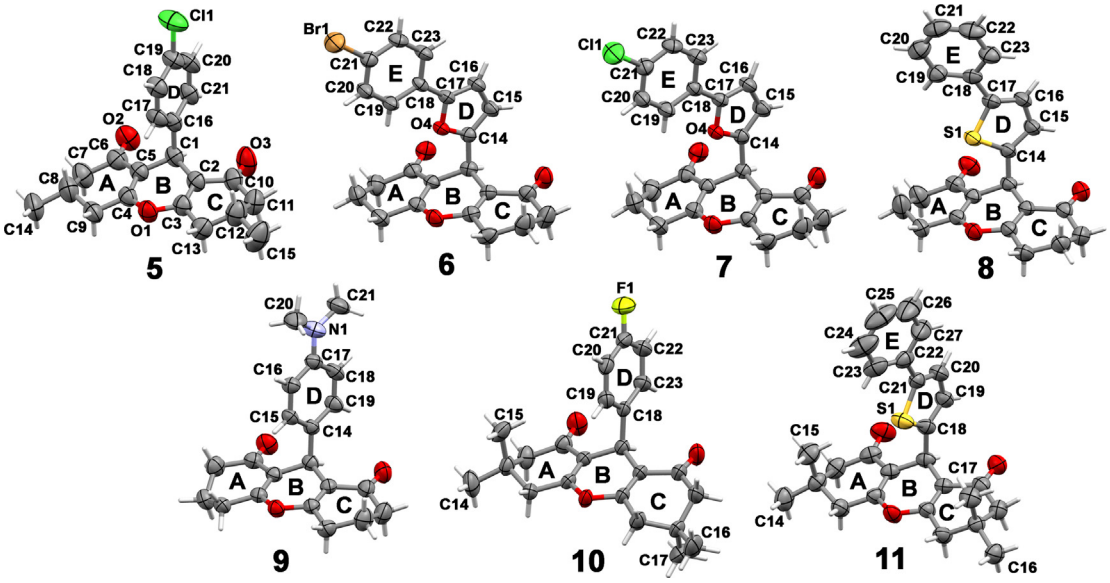

Fig. 2 50% ellipsoid plot of the non-hydrogen atoms in the asymmetric units of compounds **5**–**11** elucidated by the single-crystal X-ray diffraction technique. The labeling scheme of the rings as well as non-hydrogen atom numbering follow those shown for compound **5**.

Table 2 Selected torsion angles describing the conformation of the substituent at C1 and descriptors for half-chair conformation of rings A and C and for the planarity of ring B (r.m.s. deviation and carbon deviation in Å) in the xanthenodiones as determined by single-crystal X-ray diffraction.

Compound	O1-C1-CX-Y[a]/°	C8 deviation from the l.s. plane A -plane A r.m.s.d.[b]/Å	C12 deviation from the l.s. plane C - plane C r.m.s.d.[c]/Å	C1 deviation from the l.s. plane C - plane B r.m.s.d.[d]/Å
3[e]	−2.2(2)	0.634(2) to 0.0603	−0.596(2) to 0.0699	0.284(2) to 0.0555
4[e]	−2.2(2)	0.617(2) to 0.0557	−0.579(2) to 0.0740	0.267(2) to 0.0508
5	−7.0(3)	0.561(4) to 0.0301	0.657(4) to 0.0398	0.148(2) to 0.136
6	−26.1(4)	0.611(5) to 0.0435	0.609(5) to 0.0513	0.161(4) to 0.142
7	−25.3(2)	0.596(3) to 0.0432	0.640(3) to 0.0537	0.1599(19) to 0.145
8	−34.0(2)	0.511(4) to 0.0544	0.630(3) to 0.0588	0.166(2) to 0.146
9	−16.6(3)	−0.525(3) to 0.0649	0.601(4) to 0.0524	0.160(2) to 0.134
10	−5.3(3)	0.610(3) to 0.0614	−0.585(3) to 0.0670	0.117(2) to 0.103
11	−9.3(2)	0.634(2) to 0.0475	0.6195(19) to 0.0152	−0.1342(19) to 0.114

[a] X = 14 in 6 to 9; X = 16 in 5; X = 18 in 10 and 11; Y = S1 in 8 and 11; Y = O4 in 6 and 7; Y = C15, C17 or C19 in 9, 5 and 10.
[b] Plane A was fitted through the C9-C4-C5-C6-C7 atoms.
[c] Plane C was fitted through the C13-C3-C2-C10-C11 atoms.
[d] Plane B was fitted through the C1-C2-C3-O1-C4-C5 atoms.
[e] Geometric parameters taken from literature crystal structures (Bigdeli et al., 2007; Tu et al., 2002).

bond connecting the xanthenodione core to its substituent at C1. Such an intramolecular feature can be viewed in Fig. 3, a molecular overlay of all asymmetric units (only non-hydrogen atoms) through the xanthenodione core.

Even so, the plane of the substituent at C1 is pointed toward the ring A in all compounds, but with different bent levels. Such conformational predilection is more prominent in compounds with either furan (**6** and **7**) or thiophene (only **8**) rings attached at C1. The dihedral angle among the atoms O1, C1, CX (X = 14 in **6**–**9**; X = 16 in **5**; X = 18 in **10** and **11**) and Y (Y = S1 in **8** and **11**; Y = O4 in **6** and **7**; Y = C15, C17, or C19 in **9**, **5**, and **10**) describes this conformational feature (Table 2).

The deviation from 0° indicates that the mean plane of the substituent at C1 coinciding with the transverse plane of the xanthenodione core is more pronounced in compounds **6**–**8** than in the others. In the case of the compounds possessing furan and tiophene rings, the heteroatom of the substituent at C1 is positioned on the same side of O1, in a so-called *syn* conformation, relative to the xanthenodione core. Also in these compounds, the *para*-halogenated phenyl ring is coplanar to furan in **6** and **7** and their l.s. mean planes form angles of 2.53(11)° and 4.11(7)°, respectively. On the other hand, the non-substituted phenyl ring and thiophene are twisted in **8** and **11**, with angles of 33.08(8)° and 16.67(8)°, respectively, between their l.s. mean planes. In compound **9**, there is an electronic conjugation between the 4-*N*,*N*-dimethylamine group and the phenyl ring bonded to C1, which can be observed by looking at the coplanarity between these moieties. There is an angle of 9.3(2)° between the planes calculated through the atoms C20-N1-C21 and C14-C15-C15-C17-C18-C19 in this compound. Furthermore, ring B is slightly distorted in all structures, with C1 carbon atom as the most deviated from the l.s. mean plane through the six ring atoms (Table 2).

In all structures, only the non-classical hydrogen bonds (CH...halogen and CH...O) and other weak contacts involving π-systems (π...π, CH...π) are responsible for keeping the molecules together in the crystals. The isostructural compounds **6** and **7** are featured by alternation of the centrosymmetrically-related molecules into one-dimensional (1D) chains running parallel to the [100] direction through C7-H7A (or B in **7**)...O4, $\pi_{(ring\ D)}...\pi_{(ring\ D)}$, C12-H12A...Br (or Cl in **7**), and C8-H8B...O2 (Fig. 4).

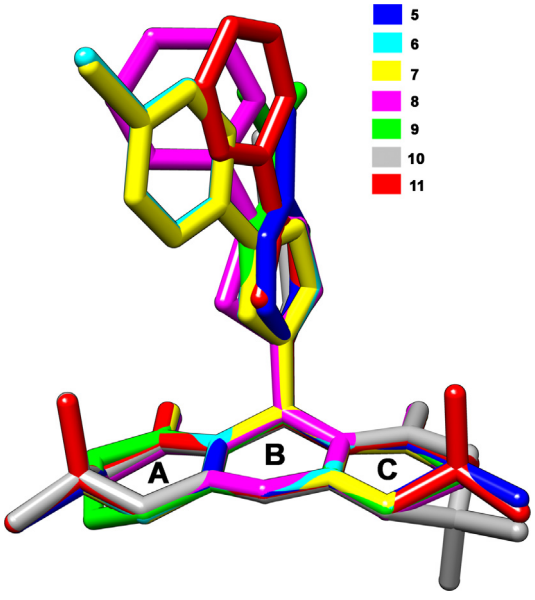

Fig. 3 Molecular overlay of all asymmetric units (only non-hydrogen atoms) through the xanthenodione core and labeling scheme of its rings.

Both carbons at the half-chair flaps are involved in the last two contacts, which can indicate a conformational adaptability from these moieties to favor geometrically the intermolecular interactions around the crystal environment. On contrary, these methylene groups do not participate significantly in the crystal packing of compound **8**. This structure is marked by formation of a centrosymmetric dimer where the CH moiety at the *para*-position of the phenyl ring is a non-classical hydrogen bonding donor to O2 (Fig. 5). This contact explains the phenyl ring twist observed in this structure. Such a phenomenon, also found in compound **11**, is a consequence of a geometrical balance to form two CH...π contacts involving the π-system of the phenyl ring E (Fig. 5).

Compounds **3**, **4**, and **10** are isostructurals as expected from their molecular similarities (differing only for the halogen at the *para*-position of the phenyl ring bonded to C1) (Fig. 6). Even though there are changes in the non-classical hydrogen bonding geometry, they keep the same main supramolecular motifs as, for instance, an 1D chain assembled through the CH...halogen contact having the methyl moiety at C12 as a donor. This chain grows along the [001] direction and is made up of *c*-glide related molecules (Fig. 6).

Crystal packing of **5** is stabilized by means of CH...O and CH...π interactions, which gives rise to chains running parallel to the [101] direction (Fig. 7).

In the crystal structure of **9**, there is formation of a 1D chain along the [010] direction where both carbonyl oxygens are non-classical hydrogen bonding acceptors from the methylene groups close to O1 (Fig. 8a). In this structure, there is also the face-to-face stacking of two centrosymmetry-related molecules through π...π interactions. This last interaction occurs between the π-system of phenyl moiety and the π-cloud around the nitrogen in the 4-*N*,*N*-dimethylamine revealing, therefore, a dual intramolecular and intermolecular conjugation phenomenon in this compound (Fig. 8b).

3.3. Theoretical aspects

The theoretical geometries of compounds **3**–**11** in the gas phase and in water are depicted in Fig. S1 (see supplementary material). In the crystal phase, molecular backbones have shown a preferential *syn* conformation for compounds **6**, **7**, **8**, and **11** regarding the O1-C1-CX-Y torsion (Y = O4 in **6** and **7**, or S1 in **8** and **11**; Fig. 9).

It is important to mention that *anti*/*syn* conformations, regarding the aforementioned dihedral, occur when the aromatic substituent is a furan or thiophene derivative (compounds **6**, **7**, **8**, and **11**). When the aromatic portion corresponds to a phenyl group, there is no differentiation considering *anti*/*syn* conformations. With no significant geometry difference between the gas phase and water, our calculations converged to similar conformations noticed in Section 3.2. Applying a conformational screening around this dihedral angle, it was possible to investigate why there is predominance

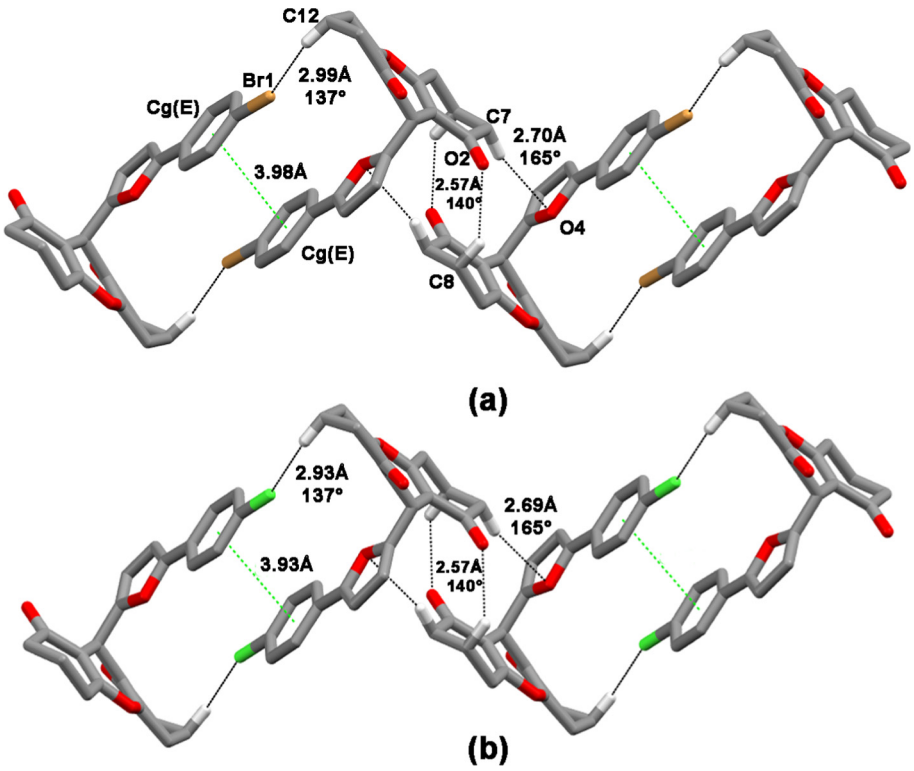

Fig. 4 Isostructural supramolecular chains in (a) **6** and (b) **7** growing parallel to the [100] direction. Cg(E) denotes the centroid calculated through ring E atoms. In this picture and hereinafter, only hydrogen atoms involved in the displayed contacts were not omitted. The depicted measurements refer to the hydrogen. . .acceptor (i. e., oxygen, halogen or Cg) distance and the weak hydrogen bonding angle. When there, Cg. . .Cg distance is also exhibited.

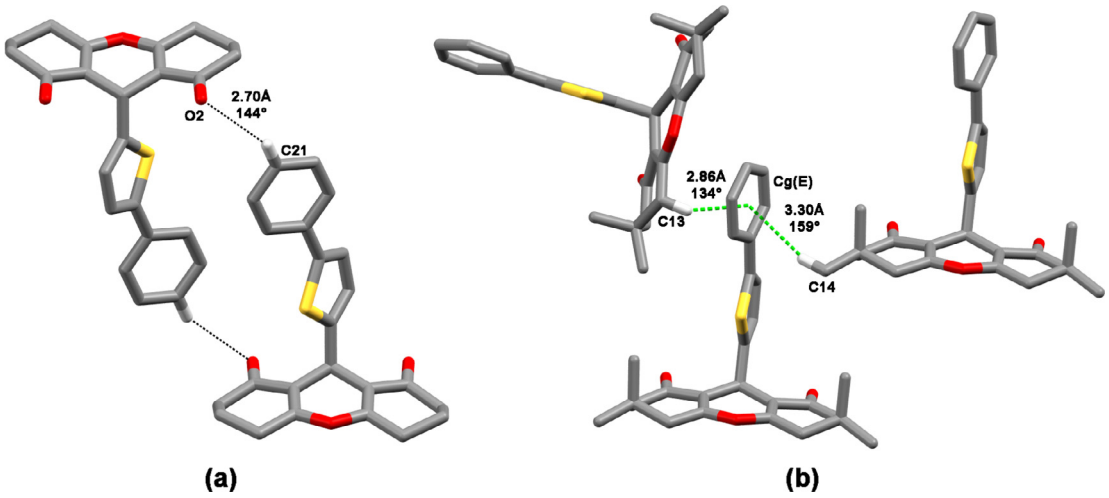

Fig. 5 The pattern of weak intermolecular contacts responsible for phenyl ring E twist in (a) **8** and (b) **11**.

for the *syn* conformations. Thus, from the optimized structure obtained by theoretical calculations, the variation of energy due to torsion of the O1-C1-CX-Y dihedral can be seen in Fig. 10. In this case, the **D** point is the energy minima and is equivalent to the optimized structure. In addition, compounds **6** and **7** have identical R' and R'' groups (Fig. 1), which result in very similar energy profiles. Because of their similarity, it is possible to discuss them together. Figs. S2 and S3 (see supplementary material) illustrate the conformers corresponding to points **A**, **B**, **C**, and **D** for compounds **6** and **7** along with some information about important dihedrals and atomic distances. The maximum energy observed in the diagrams of compounds **6** and **7** (Fig. 10) is point **A**. Comparing the structures of the conformers associated with points **A** and **B**, it is possible to recognize the fact that red eclipsed oxygens are not the main feature responsible for the higher energy of the point **A** conformer. Considering compound **6**, going from **A** to **B**, the dihedral angle decreases from 33.41° to 11.59°. This fact results in

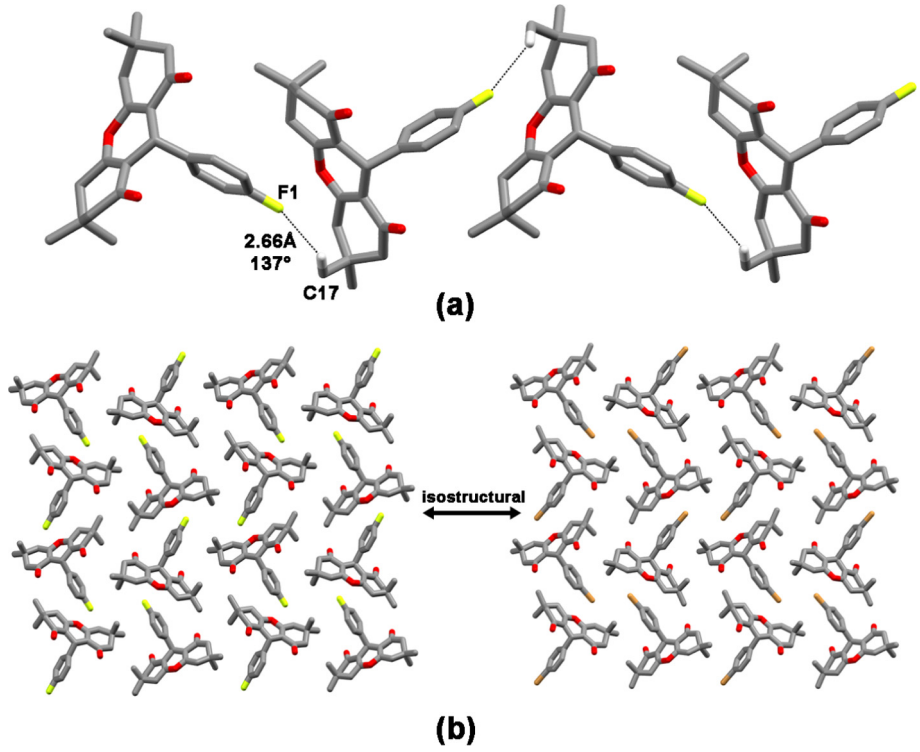

Fig. 6 (a) The supramolecular chain of **10** growing along the [001] direction. (b) Isostructural crystal packing of **10** (left) and of its bromine analog (right).

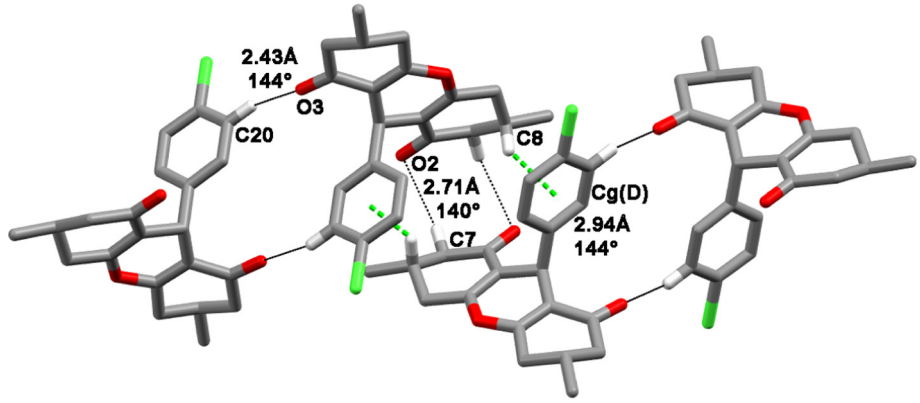

Fig. 7 Supramolecular chain running parallel to the [101] direction in compound **5**. Cg(D) denotes the centroid calculated through ring D atoms.

increased repulsion between these atoms. However, from Fig. 10, the energy decreases from points **A** to **B**. Moreover, the yellow-highlighted dihedrals also decrease from 93.34° to 48.34° for compound **6** which results an eclipsing of the oxygen and hydrogen atoms. Furthermore, the decreasing of the aforementioned dihedrals implies in approximation of oxygen and carbon atoms in the conformer related to point **A**. In this conformer, the distance between them is 2.70 Å, whereas in the point **B** conformer, it grows to 3.05 Å. Points **C** and **D** are those where two oxygens are in *anti* and *syn* conformations, respectively. The energy difference between these two points is more than 2.5 kcal·mol^{-1}. The key to understanding the higher stability of the point **D** conformer is to look at the oxygen atom of the furan ring. In the point **C** conformer, this oxygen is eclipsed by hydrogen at a distance of 2.42 Å, whereas in point **D** the closest atom to the same oxygen is a carbon at a distance of 2.92 Å. By the same reason, it is also relevant to realize that the point **C** conformer is higher in energy than that for point **B**, although the distance between the two oxygens is higher in the conformer related to the point **C**. Therefore, it is expected that compounds **6** and **7** adopt the *syn* conformation.

Figs. S4 and S5 (see supplementary material) illustrate the important aspects for the compounds **8** and **11** (Y = S1) that have differences in terms of R' and R'' groups (Fig. 1). From Fig. 10, the energy maximum for compound **11** (point **A**) is greater than 6 kcal·mol^{-1}, while for compound **8**, it is below

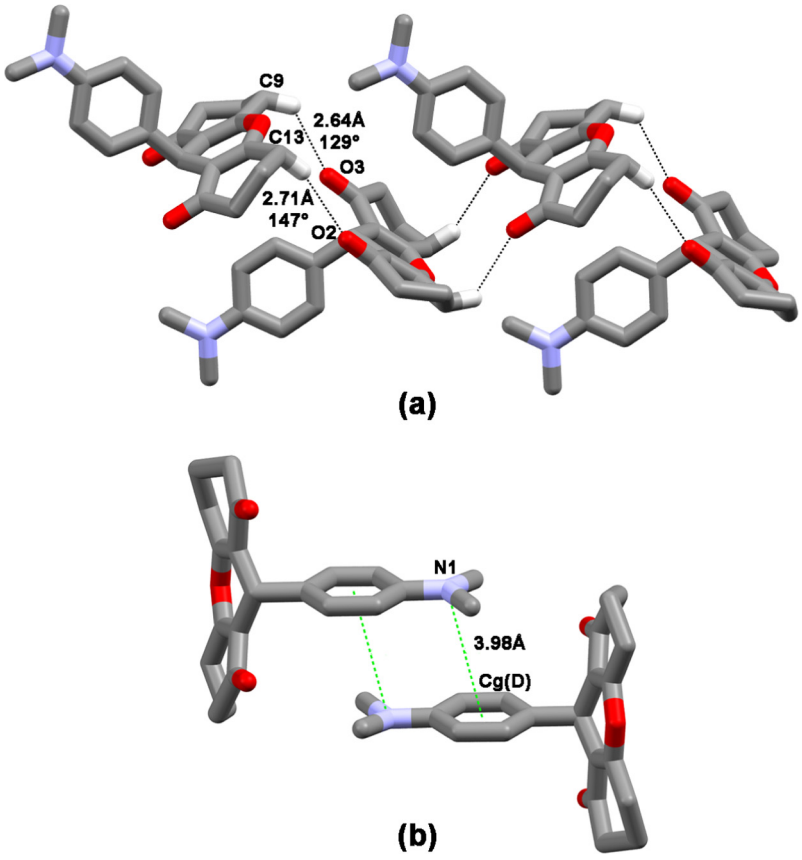

Fig. 8 (a) Supramolecular chain running parallel to the [010] direction in compound **5** and (b) the $\pi_{(N1)}\ldots\pi_{(ring\ D)}$ interactions stabilizing the centrosymmetric dimer in this structure. Cg(D) denotes the centroid calculated through ring D atoms.

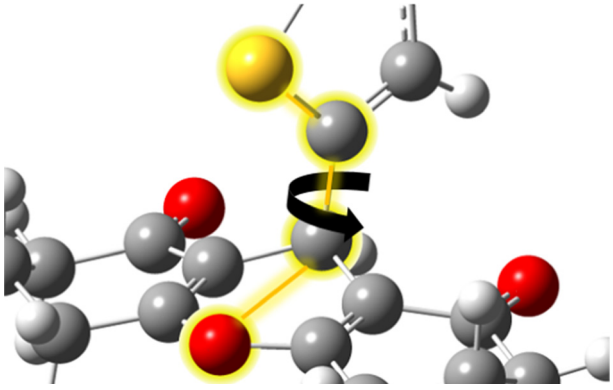

Fig. 9 O1-C1-CX-Y dihedral angle in compounds **6**, **7**, **8**, and **11** (Y = O4 in **6** and **7**, or S1 in **8** and **11)**.

4 kcal·mol^{-1}. The superior energy of the point **A** conformer of compound **11** compared to that of compound **8** was ascribed to the repulsion among the sulfur atom and methyl groups. In the point **A** conformer of compound **8**, there are two carbons which are eclipsed. However, in compound **11**, the sulfur atom is eclipsed by the carbon. Therefore, higher repulsion is expected for compound **11** regarding its point **A** conformer. However, the point **C** conformer of compound **8** has also sulfur and carbon atoms eclipsed, albeit with almost half of the point **A** destabilization energy compared to the same point of compound **11**. The reason is the existence of methyl groups in compound **11** which increase the steric repulsion, while for compound **8**, R' and R" are hydrogens (Fig. 1). To agree with this argument, an interesting effect happens considering the **11-***syn* to **11-***anti* interconversion (Fig. S1). As the O1-C1-CX-S1 dihedrals changes, one methyl group goes down through the plane to relieve the repulsion between the other CH_3 and sulfur. This same effect does not occur in the **8-***syn* to **8-***anti* interconversion since R' and R" are hydrogens (Fig. 1). In the *anti* and *syn* conformations (**B** and **D** points, respectively), it is possible to apply the same arguments used for compounds **6** and **7** to justify the preference for the *syn* conformation. In the case of compounds **8** and **11,** the reason involves the distance of sulfur to other atoms. Compounds **8** and **11** are destabilized by more than 2.0 kcal·mol^{-1}considering point **B**. For compound **8**, the sulfur atom is close to oxygen and a hydrogen by, respectively, 3.28 Å and 2.60 Å in the point **B** conformer. In the point **D** conformer, the closest sulfur distance to oxygen and carbon atoms are 3.82 Å and 3.53 Å, respectively Considering compound **11**, the respective distances are 3.31 Å and 2.79 Å for the point **B** conformer and 3.77 Å and 3.55 Å for the point **D** conformer. In both cases, in the *anti*-conformer, the repulsions are more severe than in the *syn* conformation. Thus, the *syn* conformer predominates for both compounds.

Crystal structure analyses have also revealed two distinct conformational preferences for the cyclohex-2-enone moieties of compounds **3**–**11**. Compounds **3**, **4**, **9**, **10**, and **12** adopt the *anti* conformation, while compounds **5**, **6**, **7**, **8**, and **11**

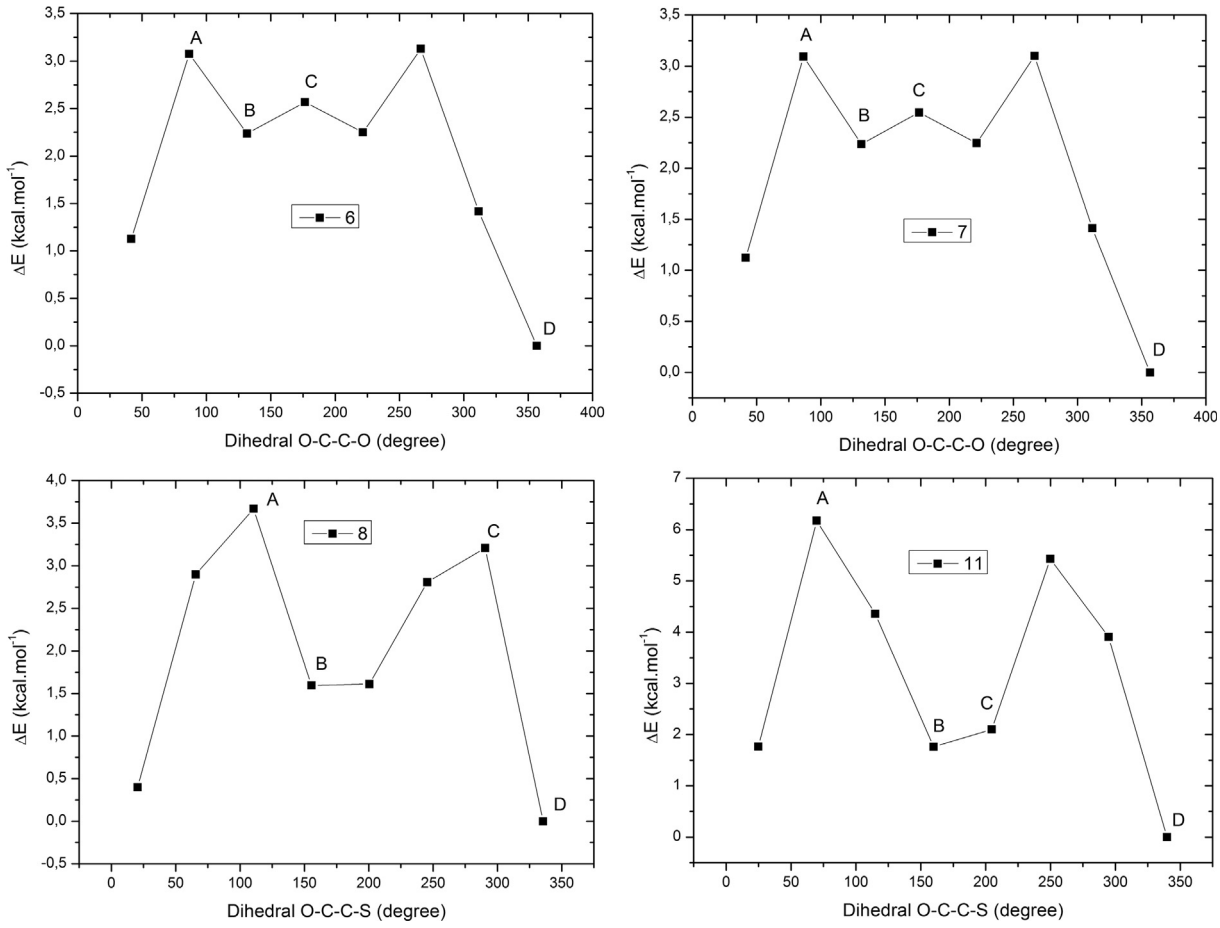

Fig. 10 Potential energy curves from the conformational analyses of compounds **6**, **7**, **8** and **11**.

assume the *syn* conformation. The geometries of all conformations can be seen in Fig. S1 (see supplementary material). Table 3 shows the energy barrier of a possible interconversion between the *syn* and *anti* conformations following the equation:

$$\Delta E = E_{syn} - E_{anti} \quad (1)$$

Applying Eq. (1) for the compounds **3**–**11**, energies were calculated from frozen crystal coordinates, enforcing only their respective opposite cyclohex-2-enone *syn* or *anti* conformer. The obtained ΔE values for **3**, **9**, **10**, and **12** were positive due to the higher stability (and therefore lower energy values) of *anti* conformers. However, our calculations in the gas phase and in water predicts that *syn* conformers are electronically more stable for all compounds (ΔE < 0). In fact, for an isolated or solvated molecule, these compounds might exist in a *syn* conformer, which disagrees with the experimental data. This difference might be due to the supramolecular contributions (see Fig. 11).

Fig. 11 shows the built dimmers of compounds **3**, **7**, **11**, and **12** that were taken as models to understand the solid-state data through the supramolecular model. These dimmers were built following the crystal coordinates. To obtain the hypothetic *syn*/*anti* conformers, the dimmers were optimized using molecular mechanics (UFF) with the aromatic groups frozen. The energy was calculated with a single-point at the ωb97xD/6-31 1++** level. All aromatic groups have aromaticity and conjugated bonds, and molecules with *syn*-orientation can potentially perform stacked interactions, such as π-π*-stacking and T-shaped, which have strong dispersive and charge transfer

Table 3 *Syn-anti* interconversion electronic energy barrier (kcal·mol^{-1}) for the cyclohexenone moiety conformation in gas phase at 25 °C (Gp) and water at 85 °C, and in gas phase dimmers (Gp Dim) at 25° (see Fig. 11 for dimmers).

ΔE	3[a]	5	6	7	8	9	10	11	12
Gp	−0.68	−0.91	−0.47	−0.49	−0.44	−0.37	−0.71	−0.48	−0.61
Water	−0.65	−0.96	−0.56	−0.58	−0.53	−0.45	−0.69	−0.57	−0.56
Gp Dim	1.66	–	–	−1.98	–	–	–	−0.82	0.63

[a] Since crystal structure of both related compounds **3** and **4** had been determined previously, in this calculation we have selected only compound **3** to represent these halogenated xanthenodiones.

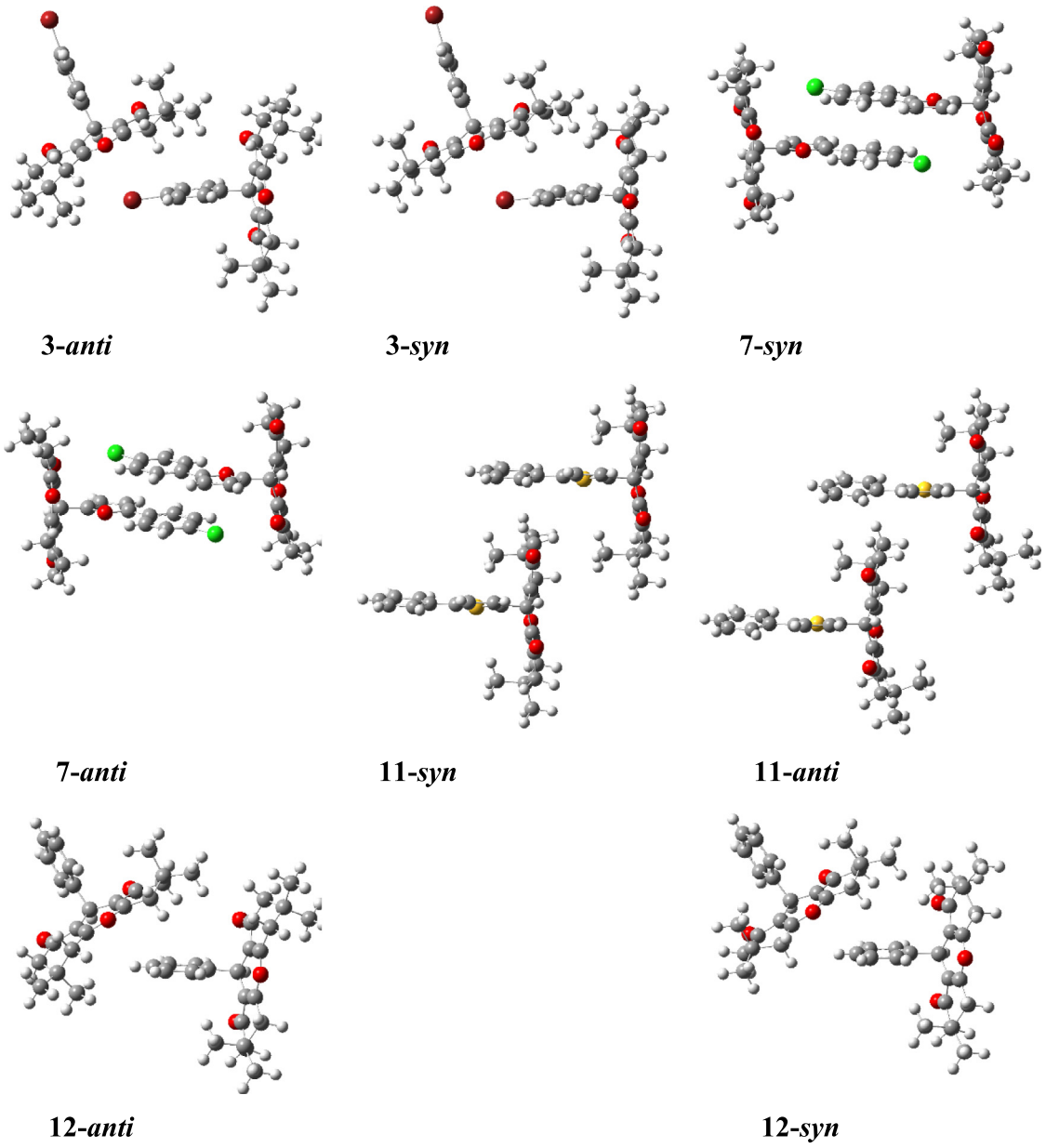

Fig. 11 Calculated gas phase geometries of the dimmers with either s*yn* or *anti* cyclohex-2-enone rings conformation.

effects that can only be described by suitable quantum mechanics methods (Josa et al., 2014a; Ramalho et al., 2013; Quin and Tyrell, 2010). The interaction energy of each dimmer was obtained by using (2), where A and B are the monomers. Table 3 also shows the interconversion energy barrier between the *syn*/*anti* dimmers in the gas phase (3).

$$\Delta E_{int} = E^{AB} - (E^{A} + E^{B}) \quad (2)$$

$$\Delta E = \Delta E_{int/syn} - \Delta E_{int/anti} \quad (3)$$

Even though it is not identical to the solid state, the supramolecular approach with two monomers have already demonstrated to agree with the experimental data. The ΔE for compounds **3** and **12** present a positive signal indicating that *anti* conformation is indeed preferred. The calculation results for compounds **7** and **11** have kept the preference for the *syn* conformations as the crystal data have shown, which is the most natural occurrence since the monomers adopt this same conformation. One interesting question is why did the conformational change happen in compounds **3**, **4**, **9**, **10**, and **12**?

Looking at the geometries of the compound **7** dimmers (Fig. 11), it is possible to see that parallel displaced π-π*-stacking rules the interaction between the monomers. Even just changing the hydrogens position between its *syn* and *anti* conformations, the energy barrier is -1.98 kcal·mol^{-1}, while the ΔE between the monomers was just -0.09 kcal·mol^{-1} in the gas phase. In this case, the dispersive interactions between Cl and H could be decisive to stabilize the supramolecule along with the stacking interactions.

With a short-conjugated chain and a large substituent as bromine, compound **3** cannot perform π-π*-stacking but angular T-shaped $\sigma_{C\text{-}H} \rightarrow \pi^*_{Ar}$ and dispersion interactions (Josa et al., 2014b; Santos et al. 2014). In its *syn* conformation, the methyl group can make these interactions difficult, increasing the system steric repulsion. In addition, the methyl group, oriented on the same side of the aromatic group in **3**-*anti*, contributes to increasing the dispersion interactions with bromine. This fact can be supported by comparing the dimmers of compounds **3** and **12**, whose ΔE values are 1.66 kcal·mol^{-1} and 0.63 kcal·mol^{-1}, respectively. The ΔE in the gas phase between their monomers were almost the same, −0.68 kcal·mol^{-1} for compound **3** and −0.61 kcal·mol^{-1} for compound **12**, which means that somehow the **3**-*anti* dimmer is more stabilized than the **12**-*anti* dimmer.

The crystal data and the theoretical calculations for compound **11** have also revealed possible T-shaped $\sigma_{C\text{-}H} \rightarrow \pi^*_{Ar}$ interactions in the dimmers of compound **11**. However, the dispersion can also be important. The ΔE for the monomers is −0.48 kcal·mol^{-1} and −0.82 kcal·mol^{-1} for the dimmer. This gain in the stabilization energy can be correlated to the C—H and methyl group dispersive interactions, which are completely erased in the **11**-*anti* dimmer. In this prospect, our findings highlight the importance of the intermolecular interactions in this conformational preference. Indeed, intermolecular interactions are crucial for the solid state matter (Pereira et al., 2011) and it can show more distinct behavior than the solvated molecule if non-classical effects are considered, which can be easily understood with the supramolecular approach. It is worth emphasizing that all these interactions in the dimmer state can be intensified in the solid state by increasing the number of monomers present in the supramolecule.

4. Conclusions

In this investigation, a series of nine 1,8-dioxooctahydroxanthenes, which have been rarely studied from a structural point of view, were synthesized and had their structures investigated. It was described, for the first time, the crystal structures of seven of the prepared compounds. We have interpreted the changes in their conformation based on the energetic profiles of the single molecules and dimers, highlighting the prevalence of intramolecular forces in the *anti* conformation of the C1 substituent, common to all compounds. Likewise, intermolecular forces drive the *anti* conformation of the cyclohex-2-enone half-chair moieties. Based on this study, we hope that similar correlated experimental–theoretical investigations can be performed with other xanthenodione compounds to find other examples and exceptions of these supramolecular and conformational features of this class compound, which can impact their biological and physicochemical properties.

Acknowledgments

We are grateful to Fundação de Amparo à Pesquisa do Estado de Minas Gerais (FAPEMIG-CEX APQ 01287/14), Coordenação de Aperfeiçoamento de Pessoal de Nível Superior (CAPES) and Conselho Nacional de Desenvolvimento Científico e Tecnológico (CNPq) for financial support.

Appendix A. Supplementary material

Supplementary data associated with this article can be found, in the online version, at http://dx.doi.org/10.1016/j.arabjc.2017.09.001.

References

Baltork, I.M., Khosropur, A.R., Hojati, S.F., 2007. $ZrOCl_2{\cdot}8H_2O$ as an environmentally friendly and recyclable catalyst for the chemoselective synthesis of 2-aryloxazolines and bis-oxazolines under thermal conditions and microwave irradiation. Catal. Commun. 8, 200–204.

Banerjee, A., Mukherjee, A.K., 1981. Chemical aspects of santalin as a histological stain. Stain Technol. 56, 83–85.

Banerjee, A.G., Kothapalli, L.P., Sharma, P.A., Thomas, A.B., Nanda, R.K., Shrivastava, S.K., Khatanglekar, V.V., 2016. A facile microwave assisted one pot synthesis of novel xanthene derivatives as potential anti-inflammatory and analgesic agents. Arabian J. Chem. 9, S480–S489.

Bardajee, G.R., 2013. C. R. $ZrOCl_2{\cdot}8H_2O$ in water: An efficient catalyst for rapid one-pot synthesis of pyridopyrazines, pyrazines and 2,3-disubstituted quinoxalines. Chimie 16, 872–877.

Bigdeli, M.A., Mahdavinia, G.H., Amani, V., 2007. 9-(4-Bromophenyl)-3,3,6,6-tetramethyl-3,4,6,7-tetrahydro-2H-xanthene-1,8(5H,9H)-dione. Acta. Crystallogr. Sect. E 63, o3493.

Bruker, 2012. SAINT Program for Data Reduction from Area Detectors. BRUKER AXS Inc., 5465 East Cheryl Parkway, Madison, WI 53711-5373 USA.

Callan, J.F., De Silva, P., Magri, D.C., 2005. Luminescent sensors and switches in the early 21st century. Tetrahedron 61, 8551–8588.

Dua, R., Shrivastava, S., Sonwane, S.K., Shrivastava, S.K., 2011. Pharmacological significance of synthetic heterocycles scaffold: a review. Advan. Biol. Res. 5, 120–144.

Frisch, M.J., Trucks, G.W., Schlegel, H.B., Scuseria, G.E., Robb, M. A., Cheeseman, J.R., Scalmani, G., Barone, V., Mennucci, B., Petersson, G.A., Nakatsuji, H., Caricato, M., Li, X., Hratchian, H. P., Izmaylov, A.F., Bloino, J., Zheng, G., Sonnenberg, J.L., Hada, M., Ehara, M., Toyota, K., Fukuda, R., Hasegawa, J., Ishida, M., Nakajima, T., Honda, Y., Kitao, O., Nakai, H., Vreven, T., Montgomery, J.A., Jr., Peralta, J.E., Ogliaro, F., Bearpark, M., Heyd, J.J., Brothers, E., Kudin, K.N., Staroverov, V.N., Kobayashi, R., Normand, J., Raghavachari, K., Rendell, A., Burant, J.C., Iyengar, S.S., Tomasi, J., Cossi, M., Rega, N., Millam, J.M., Klene, M., Knox, J.E., Cross, J.B., Bakken, V., Adamo, C., Jaramillo, J., Gomperts, R., Stratmann, R.E., Yazyev, O., Austin, A.J., Cammi, R., Pomelli, C., Ochterski, J.W., Martin, R.L., Morokuma, K., Zakrzewski, V.G., Voth, G.A., Salvador, P., Dannenberg, J.J., Dapprich, S., Daniels, A.D., Farkas, Ö., Foresman, J.B., Ortiz, J. V., Cioslowski, J., Fox, D.J., 2009. Gaussian, Inc., Wallingford CT.

Hafez, E.A.A., Elnagdi, M.H., Elagamey, A.G.A., El-Taweel, F.M.A. A., 1987. Cycloaddition reaction of 1,2,4-trazolium phenacylides with cinnamic esters. Heterocycl. 26, 903–907.

Ilangovan, A., Malayappasamy, S., Muralidharan, S., Maruthamuthu, S., 2011. A highly efficient green synthesis of 1, 8-dioxooctahydroxanthenes. Chem. Cent. J. 5, 81.

Ion, R.M., Frackowiak, D., Planner, A., Wiktorowicz, K., 1998. The incorporation of various porphyrins into blood cells measured *via* flow cytometry, absorption and emission spectroscopy. Acta. Biochim. Pol. 45, 833–845.

Josa, D., dos Santos, L.A., Gonzalez-Veloso, I., Rodriguez-Otero, J., Cabaleiro-Lago, E.M., Ramalho, T.C., 2014a. Ring-annelated corannulenes as fullerene receptors. A DFT-D study. RSC Adv. 4, 29826–29833.

Josa, D., Rodriguez-Otero, J., Cabaleiro-lago, E.M., Santos, L.A., Ramalho, T.C., 2014b. Substituted corannulenes and sumanenes as

fullerene receptors: a dispersion-corrected density funtional theory study. J. Phys. Chem. A 118, 9521–9528.

Kalantari, M., 2012. Synthesis of 1,8-dioxo-octahydroxanthenes and bis(indoyl)methanes catalyzed by $[Et_3NH][H_2PO_4]$ as a cheap and mild acid ionic liquid. Arab. J. Chem. 5, 31–39.

Kumar, G.S.S., Prabhu, A.A.M., Seethalashmi, P.G., Bhuvanesh, N., Kumaresan, S., 2014. Self-catalyzed syntheses, structural characterization, DPPH radical scavenging-, cytotoxicity-, and DFT studies of phenoxyaliphatic acids of 1,8-dioxo-octahydroxanthene derivatives. J. Mol. Struct. 1059, 51–60.

Lamberth, C., Dinges, J. (Eds.), 2012a. Bioactive Heterocyclic Compound Classes: Pharmaceuticals. Wiley-VCH Verlag & Co., Weinheim, Germany.

Lamberth, C., Dinges, J. (Eds.), 2012b. Bioactive Heterocyclic Compound Classes: Agrochemicals. Wiley-VCH Verlag & Co., Weinheim, Germany.

Macrae, C.F., Bruno, I.J., Chisholm, J.A., Edgington, P.R., Mccabe, P., Pidock, E., Monge, L.R., Taylor, R., van de Streek, J., Wood, P.A., 2008. Mercury CSD 2.0 – new features for the visualization and investigation of crystal structures. J. Appl. Crystallogr. 41, 466–470.

Mosaddegh, E., Islami, M.R., Hassankhani, A., 2012. $ZrOCl_2.8H_2O$ as an efficient and recyclable catalyst for the clean synthesis of xanthenedione derivatives under solvent-free conditions. Arab. J. Chem. 5, 77–80.

Mulakayala, N., Murthy, P.V.N.S., Rambabu, D., Aeluri, M., Adepu, R., Krishna, G.R., Reddy, C.M., Prasad, K.R.S., Chaitanya, M., Kumar, C.S., Rao, M.V.B., Pal, M., 2012. Catalysis by molecular iodine: A rapid synthesis of 1,8-dioxo-octahydroxanthenes and their evaluation as potential anticancer agents. Bioorg. Med. Chem. Lett. 22, 2186–2191.

Naidu, K.R.M., Krishna, B.S., Kumar, M.A., Arulselvan, P., Khalivulla, S.I., Lasekan, O., 2012. Design, synthesis and antiviral potential of 14-aryl/heteroaryl-14*H*-dibenzo*[a, j]*xanthenes using an efficient polymer-supported catalyst. Molecules 17, 7543–7555.

Nisar, M., Ali, I., Shah, M.R., Badshah, A., Qayum, M., Khan, H., Khan, I., Ali, S., 2013. Amberlite IR-120H as a recyclable catalyst for the synthesis of 1,8-dioxo-octahydroxanthene analogs and their evaluation as potential leishmanicidal agents. RSC. Adv. 3, 21753–21758.

Obi-Egbedi, N.O., Obot, I.B., 2012. Adsorption behavior and corrosion inhibitive potential of xanthene on mild stell/sulphuric acid interface. Arab. J. Chem. 5, 121–133.

Omolo, J.J., Johnson, M.M., Vuuren, S.F.V., de Koning, C.B., 2011. The synthesis of xanthones, xanthenediones, and spirobenzofurans: Their antibacterial and antifungal activity. Bioorg. Med. Chem. Lett. 21, 7085–7088.

Pereira, M.C., Garcia, E.M., da Silva, A.C., Lorençon, E., Ardisson, J. D., Murad, E., Fabris, J.D., Matencio, T., Ramalho, T.C., Rocha, M.V.J., 2011. Nanostructured d-FeOOH: A novel photocatalyst for water splitting. J. Mater. Chem. 21, 10280–10282.

Pirouzmand, M., Gharehbaba, A.M., Ghasemi, Z., 2017. CTA]Fe/MCM-41: An efficiente and reusable catalyst for green synthesis of xanthene derivatives. Arab. J. Chem. 10 (8), 1070–1076. https://doi.org/10.1016/j.arabjc.2016.06.017.

Poupelin, J.P., Saint-Ruf, G., Foussard-Blanpin, O., Narcisse, G., Uchida-Ernouf, G., Lacroix, R., 1978. Synthesis and ati-inflammatory properties of bis (2-hydroxy-1-naphthyl) methane derivatives. Eur. J. Med. Chem. 13, 67–71.

Quin, L.D., Tyrell, J.A., 2010. Fundamentals of Heterocyclic Chemistry: Importance in Nature and in the Synthesis of Pharmaceuticals. John Wiley & Sons, Hoboken, New Jersey.

Ramalho, T.C., Santos, L.A., da Cunha, E.F.J., 2013. Thermodynamic framework of hydrophobic/electrostatic interactions. Biomol. Struct. Dyn. 31, 995–1000.

Reddy, B.P., Vijayakumar, V., Narasimhamurthy, T., Suresh, J., Lakshman, P.L.N., 2009. 3,3,6,6-Tetramethyl-9-phenyl-3,4,5,6-tetrahydro-9H-xanthene-1,8(2H,7H)- dione. Acta. Crystallogr. Sect. E 65, o916.

Sangshetti, J.N., Kokare, N.D., Kotharkar, S.A., Shinde, D.B., 2008. $ZrOCl_2{\cdot}8H_2O$ catalyzed one-pot synthesis of 2,4,5-triaryl-1H-imidazoles and substituted 1,4-di(4,5-diphenylimidazol-yl)benzene. Chin. Chem. Lett. 19, 762–766.

Santos, L.A., da Cunha, E.F.F., Freitas, M.P., Ramalho, T.C., 2014. Hydrophobic noncovalent interactions of inosine-phenylalanine: a theoretical model for investigating the molecular recognition of nucleobases. J. Phys. Chem. A 118. 5808–5017.

Sheldrick, G.M., 2008. A short history of SHELX. Acta. Crystallogr. Sect. A. 64, 112–122.

Tu, S., Zhou, J., Lu, Z., Deng, X., Shi, D., Wang, S., 2002. Condensation of aromatic aldehydes with 5,5-dimethyl 1,3-cyclohexanedione without catalyst. Synth. Commun. 32, 3063–3067.

Wang, H., Lu, L., Zhu, S., Li, Y., Cai, W., 2006. The phototoxicity of xanthene derivatives against *Escherichia coli*, *Staphylococcus aureus* and *Saccharomyces cerevisiae*. Curr. Microbiol. 52, 1–5.

Ziarani, G.M., Badiei, A.-R., Azizi, M., 2011. The one-pot synthesis of 14-aryl-14H-dibenzo[a, j]xanthene derivatives using sulfonic acid functionalizd sílica (SiO_2-Pr-SO_3H) under solvent free conditions. Sci. Iran. C 18, 453–457.